Lattice dynamics of skutterudites: First-principles and model calculations for $CoSb_3$

J. L. Feldman and D. J. Singh
Complex Systems Theory Branch, Naval Research Laboratory, Washington, DC 20375
(Received 11 September 1995)

The lattice dynamics of skutterudite structure $CoSb_3$ are investigated by local-density frozen phonon calculations and force-constant model fits to both the results of these calculations and experimental frequencies. First-principles calculations of the normal modes and frequencies are reported for the Γ-point A_g Raman and A_u phonons, as well as the constrained bulk modulus and its pressure derivatives. Cubic anharmonic terms are reported for the A_g modes. Comparison of the results with an existing bond-stretching force-constant model reveals poor agreement for the lowest frequency A_u phonon, whose displacement pattern is dominated by bond angle modulation with only small bond length changes. This lack of agreement is probably related to the highly covalent bonding of the material and the absence of bond angle force constants in the model. Improved force-constant models, which include bond angle forces and reproduce both the first-principles and experimental phonon frequencies, were developed. Phonon-dispersion curves and densities of states are reported along with elastic constants and the Debye temperature.

I. INTRODUCTION

There has been a renewed interest in thermoelectric materials. This is part of an overall interest in nonconventional refrigeration technologies, driven by environmental concerns related to CFC use. The main drawback of thermoelectric refrigerators is their low-energy efficiency, which is related to the performance of known thermoelectric materials. This is quantified by a figure of merit,

$$Z=\frac{\sigma S^2}{\kappa}, \tag{1}$$

where σ is the electrical conductivity, S is the Seebeck coefficient, and κ is the thermal conductivity, which has both electronic and lattice components, κ_e and κ_l, respectively. ZT, where T is the temperature, is dimensionless, and is slightly larger than unity for the best existing semiconductor materials.

The difficulty in finding better materials can be rationalized in terms of simple considerations, although there is no known fundamental restriction on ZT (N.B. $ZT\rightarrow\infty$ corresponds to Carnot efficiency in a refrigerator). In most materials, near room temperature, κ_e is approximately proportional to σT through the Widemann-Franz relation. If κ_l were negligible, $S\sim 160$ μV/K would be required for $ZT=1$ and $S\sim 350$ μV/K would be required for $ZT=5$. However, these high Seebeck coefficients correspond to low band fillings, which means relatively low values of σ. In this regime, the assumption that κ_e is dominant ordinarily breaks down, and instead κ_l dominates, lowering ZT. Clearly, a combination of favorable electronic properties (high mobility and effective mass to yield high σ and S) and a very low κ_l is needed. This combination leads to the consideration of crystalline solids with complex (many atoms per unit cell) structures, as they are favorable candidates for obtaining very low κ_l.[1]

One class of materials that apparently fits these criteria are the binary skutterudites, MA_3, where M is Co, Rh or Ir and A is a pnictogen. As such, these materials have been proposed and studied as potential thermoelectrics.[2–5] These materials, although formed as highly crystalline compounds, have a complex structure containing large voids and four formula units per cell. Unfortunately, measurements have shown that the thermal conductivities are as much as 50 times higher than the potential minimum for this structure as defined by the minimum thermal conductivity model of Slack.[1] As a result, it is now clear that without modification they will not outperform existing thermoelectrics. Potential modifications, which have been proposed, include inserting rare earth or other atoms into the voids and chemical substitutions on the anion or cation sites. Both of these strategies have been shown to lead to strongly reduced values of κ, at least in certain cases.[6,7] It seems that these materials have the potential for high values of ZT, provided that examples can be found where κ is decreased without a large degradation in the electrical transport properties. The lattice dynamics of a material is a prerequisite for gaining a theoretical understanding of its thermal conductivity, and the focus of this paper is on a lattice-dynamical force model and phonon dispersion for $CoSb_3$. We hope to apply this in future work to a rigorous calculation of the thermal conductivity.

Of the skutterudites $CoSb_3$ is perhaps the best studied in regard to lattice dynamics. Nonetheless, published data on the phonons in this material are scant. Infrared absorption measurements have provided experimental information on seven of the 19, distinct zone-center (Γ point) phonon frequencies. Here we report local-density approximation (LDA) calculations of additional frequencies and eigenvectors as well as some anharmonic parameters. In particular, A_g and A_u normal modes and their frequencies are determined. Also determined are certain cubic anharmonic coefficients associated with the A_g normal modes and the bulk modulus and its pressure derivative. Our theoretical results for harmonic quantities and the experimentally determined frequencies of the infrared-active modes are used to refine and test force-constant models. These in turn are used to provide information on the phonon dispersion.

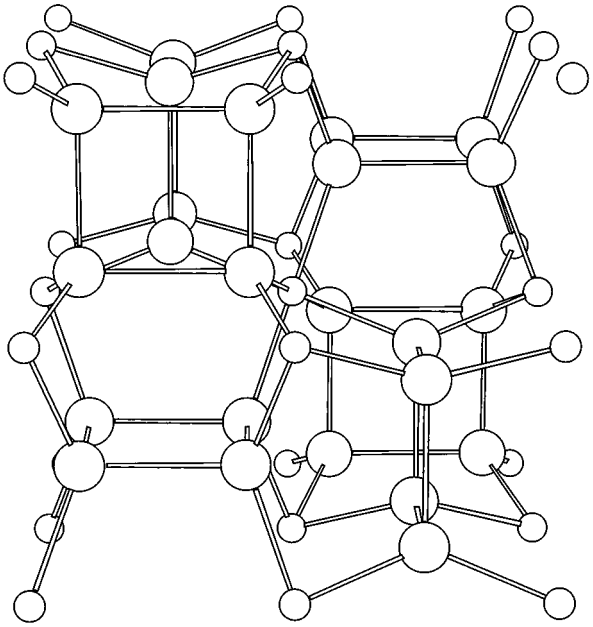

FIG. 1. Structure with bonds of strongest force-constant values connected. Co(Sb) atoms are represented by the small (large) circles.

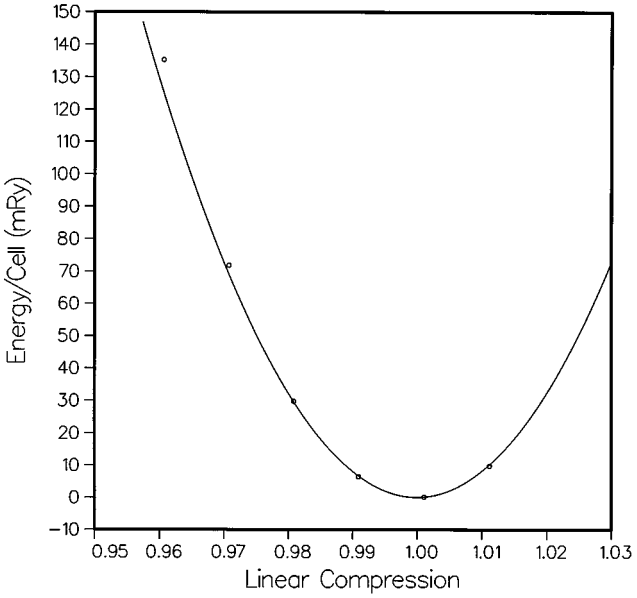

FIG. 2. LDA total energies (per bcc unit cell). Linear compression is L/L_0. Solid line gives LK model results assuming a sum of parabolic potentials with respect to the bond strains used in the LDA calculation.

The initial force-constant treatment for $CoSb_3$ is due to Lutz and Kliche (LK),[8] who fitted their six parameter central (bond-stretching) force model to infrared data. Since there are only seven distinct infrared frequencies such a model would seem unreliable at first sight. However, only one or two parameters contribute significantly to each infrared mode, as shown by LK, and the values of parameters obtained seem physically reasonable. We consider the LK model in light of our new (additional) ''data.'' Since we shall see that some embellishment of their model is necessary, a new model is introduced and rationalized. The remainder of the paper is divided as follows: Sec. II contains our LDA results, Sec. III explores various force models, Sec. IV gives phonon-dispersion curves and related functions based on those models, and Sec. V summarizes and discusses our results.

II. LDA CALCULATIONS

A. Skutterudite structure

The skutterudite structure (Fig. 1) has a bcc lattice and a basis of 4 MX_3, i.e., $CoSb_3$, formula units. It has the space group $Im3$ and two dimensionless internal parameters, u and v, that, respectively, specify the x and y spatial components of the Sb atoms. It may be conveniently regarded as consisting of an expanded (edge length $a/2=4.52$ Å) simple cubic lattice of Co atoms and four-membered rectangular, but nearly square, ''rings'' consisting of Sb atoms. The Sb_4 rings reside inside the cubes of the Co lattice, and the cubic symmetry is maintained by alternate empty and x- and y- and z-oriented Sb_4 fillings of the Co ''cubes.'' Hence of the four cubes making up the primitive unit cell, three contain Sb_4 rings and the fourth is empty. First-principles calculations[5] indicate a strongly covalent electronic structure as do small interatomic distances[9] and the existence of high hole mobilities observed in these materials.[3,4] This leads to certain expectations regarding the lattice dynamics. Strong two-body interactions can be expected between the nearest-neighbor Co and Sb atoms and between neighboring Sb atoms along the rings. Significant three-body interactions associated with these bonds, or bond-angle force constants, are typical of semiconductor lattice-dynamical models, but are not included in the Lutz-Kliche model. This may cause that model to fail for modes involving shape distortions of the Sb_4 rings and this work provides some evidence of such a failure. Futhermore, enhanced LO-TO splittings and Born effective charges e^* are expected due to the covalency; these should not be regarded as similar to ionic charges or as giving an indication of substantial ionicity in these compounds. Finally, it is worth pointing out that although much attention has been given to the Sb four-membered ring structure, Fig. 1 clearly indicates the presence of other rings such as the five- and six-membered rings involving presumably strong bonded Co and Sb atoms.

TABLE I. A_g symmetry LDA results at the experimental volume (in Ry/unit cell). Least-squares fit results for $a_{vv}=\partial^2 E/\partial^2 v$, $a_{uuv}=\partial^3 E/\partial^2 u\,\partial v$, etc. Values in the first column are the coefficients in an expansion of the total energy in powers of $u-0.335\,37$ and $v-0.157\,88$. Minimum energy values of u and v, were found to be 0.333 10 and 0.1598, respectively, and the corresponding minimum energy was found to be -3.7 mRy (relative to the energy at the experimental u,v). Values in the second column are coefficients in an expansion in powers of $u-0.333\,10$ and $v-0.1598$.

a_{uu}	730	661
a_{vv}	1025	937
a_{uv}	−29	−29
$a^*_{uuu}\times10^{-4}$	3.0	3.0
$a^*_{vvv}\times10^{-4}$	−4.6	−4.6
$a^*_{uuv}\times10^{-4}$	−0.06	−0.06
$a^*_{uvv}\times10^{-4}$	−0.03	−0.03

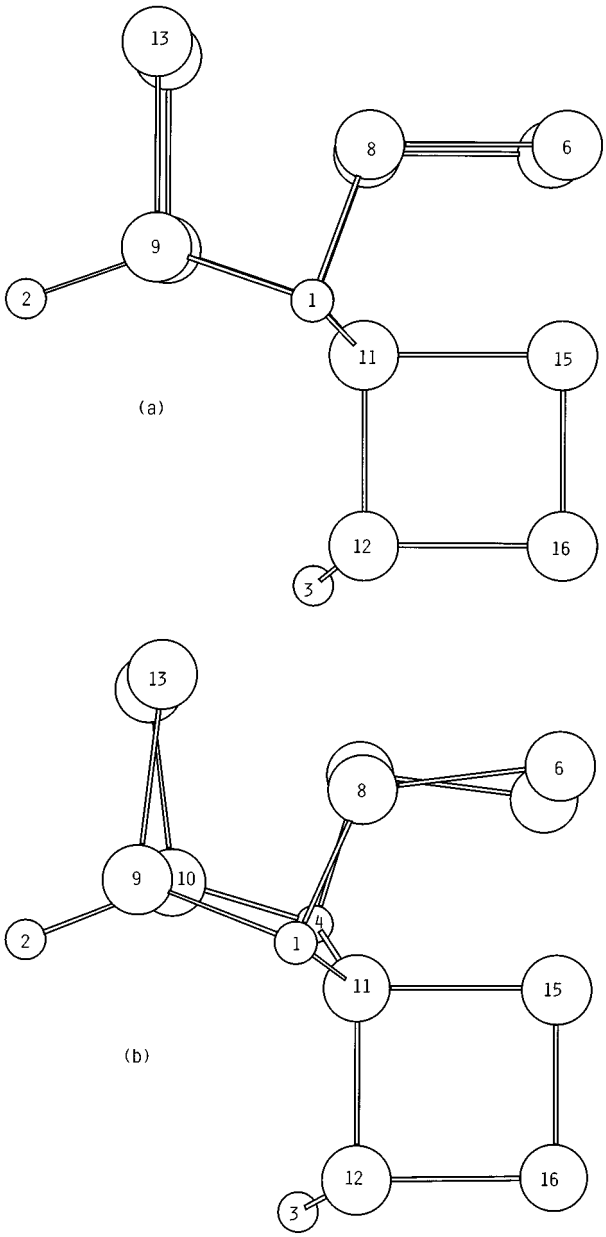

FIG. 3. A_u symmetry distortion. (a) the undistorted structure. (b) the distorted structure. The distortion corresponds to the low-frequency mode. Co (Sb) atoms are represented by small (large) circles. For reference to Table V the $x(y)$ coordinate axis is along the horizontal (vertical) and the distance between atoms 11 and 15 is the longer of the two sides of a four-membered ring.

B. Methods and bulk properties

These calculations were performed, as in other calculations for skutterudites by one of us,[5] using a local orbital extension[10] of the general potential linearized augmented plane-wave (LAPW) method.[11,12] Well converged basis sets consisting of over 3000 LAPW basis functions were employed with LAPW sphere radii of 2.2 a.u. for both Co and Sb. Local orbitals were used to relax any linearization errors and to include the Sb semicore d states on the same footing as the valence states. Both the core and valence states were treated self-consistently, the core states relativistically, and the valence states in a scalar relativistic framework. The Hedin-Lundqvist exchange-correlation parametrization[13] was used. The Brillouin-zone sampling during the iterations to self-consistency was performed using special **k** point sets. A set of eight points in the irreducible 1/48 of the zone was used for the cubic symmetry cells (bulk properties and A_g distortions), while a smaller but still well converged set of five points was used for the A_u modes (N.B. there are 16 atoms in the unit cell).

The lattice parameter, bulk modulus, and the pressure derivative of the bulk modulus were determined by the standard procedure of computing the total energy for a range of volumes and fitting to the Birch equation of state. The two internal structural parameters were not ''relaxed'' but kept fixed at their experimental zero pressure, room-temperature values, $u_e(=0.335\ 37)$ and $v_e(=0.157\ 88)$. This means that the computed LDA bulk modulus given here is not precisely the physical bulk modulus. The models may then be used to determine the physical bulk modulus and the pressure dependence of u and v. Nonetheless, this difference is expected to be small in the skutterudite structure where these parameters show only weak variation among the known compounds

TABLE II. Model parameters and elastic properties. Units: a_1–a_6, in 10^4 dyn/cm, a_7 and a_8 in 10^{-12} erg, c_{ij} and B (bulk modulus) in 10^{11} dyn/cm^2.

Par./Model	LK	*A*	*B*	*C*	*D*
a_1	8.5	7.058	6.662	6.612	6.358
a_2	0.9	1.021	0.682	1.281	0.852
a_3	8.7	7.717	7.268	7.701	7.221
a_4	5.9	5.272	5.134	5.362	5.311
a_5	2.8	2.242	2.276	2.207	2.274
a_6	1.4	0.718	0.585	0.500	0.334
a_7	0	1.311	0.606	1.456	0.912
a_g/a_7		0.46	0.46	1.000	1.000
a_9/a_1	0	0.1	0.2	0.1	0.2
c_{11}	21.3	20.2	20.5	19.8	19.9
c'	8.07	7.31	6.95	7.39	6.95
c_{44}	2.22	4.22	4.77	4.35	4.88
B	10.5	10.4	11.3	9.92	10.6
B(unrelaxed)	10.6	10.6	11.8	10.2	11.3
Debye Temp. (K)	170	205	211	207	212

TABLE III. Fitted zone-center frequencies (units: 1/cm). The experimental values given in the last column are from Ref. 8 and the LDA values, in parenthesis, are those presented in this paper.

Mode/Model	LK	*A*	*B*	*C*	*D*	Expt. (LDA)
A_g	162.1	150.5	149.7	149.3	148.4	(150.2)
	183.0	177.5	176.7	176.9	176.5	(178.5)
A_u	69.5	109.8	110.3	109.0	111.8	(109.5)
	250.4	240.0	235.6	242.4	237.2	(240.5)
F_u	79.3	77.9	78.4	78.4	77.4	78.0
	118.8	120.0	119.7	120.0	119.9	120.0
	142.6	143.8	144.6	145.0	145.9	144.0
	174.4	175.1	175.7	175.7	176.0	174.0
	241.9	240.7	237.8	241.9	239.5	247.0
	257.7	261.2	264.2	260.2	263.1	257.0
	276.9	276.8	279.9	274.8	277.8	275.0

TABLE IV. Predicted mode frequencies (zone center) (units: 1/cm).

Mode/Model	LK	*A*	*B*	*C*	*D*
E_g	139.7	138.7	140.9	140.6	142.8
	194.0	182.5	180.1	180.5	178.3
F_g	70.5	83.3	86.1	83.6	84.9
	102.9	97.1	98.0	95.6	97.4
	161.6	156.7	152.4	158.1	154.1
	188.1	178.2	172.7	176.0	171.8
E_u	94.6	130.5	137.8	138.8	144.5
	275.0	267.4	265.7	261.5	262.3

(CoP_3, $CoAs_3$, $CoSb_3$ RhP_3, $RhAs_3$, $RhSb_3$, IrP_3, $IrAs_3$, and $IrSb_3$), even though there are large variations in cell volume and ionic radii. The present calculations yield a lattice parameter of 8.937 Å, which is 1.1% smaller than the measured (room-temperature) value, as is typical in LDA calculations. The constrained bulk modulus is 105 GPa, with a pressure derivative of 4.3. The energy at the theoretical lattice parameter was found to be below that at the experimental volume by 9.7 mRy. The results are displayed in Fig. 2. The results obtained by writing the energy as a sum of quadratic terms in the changes in the interatomic distances and making use of the LK model are also shown and it is seen that the LK model predicts the LDA volume-dependent energy remarkably well. The difference between the LK results and our LDA results is primarily an anharmonic effect.

C. A_g symmetry displacements

Changes in u and v from their equilibrium values can be identified as the two A_g symmetry coordinates.[14] Calculations of the total energy were carried out at the experimental volume and thirteen (u,v)'s within 0.005 of (u_e,v_e). This maximum variation was expected to be large enough to provide information on cubic anharmonic terms and small enough to make higher-order terms negligible. Next, a least-squares fit of the results was made to an expansion in $(u-u_e,\ v-v_e)$ keeping all allowable linear, quadratic, and cubic terms; quartic terms were considered briefly, as discussed below. The fits with quartic and higher order terms set to zero corresponded to a standard deviation of 0.02 mRy and a maximum deviation of 0.06 mRy. The extracted coefficients of the linear terms in this expansion were used to obtain the theoretical equilibrium values, u_0 and v_0, and diagonalization of the 2×2 matrix, $a_{\alpha\beta}/m_{Sb}$, yielded the normal mode frequencies and polarization vectors. Due to the presence of the cubic anharmonic terms the values of the quadratic coefficients change slightly when they are defined from an expansion of the energy about u_0 and v_0, and this effect is also shown in Table I (second column). Only the former definition is employed in the remainder of this paper as, generally, LDA values of frequencies or bulk moduli based on experimental structural parameters are most accurate. The quadratic coefficients of Table I (first column) lead to normal mode frequencies of 150 and 178 cm^{-1} and polarization vectors (to be presented later in the paper) of components nearly parallel to each rectangle's long and short

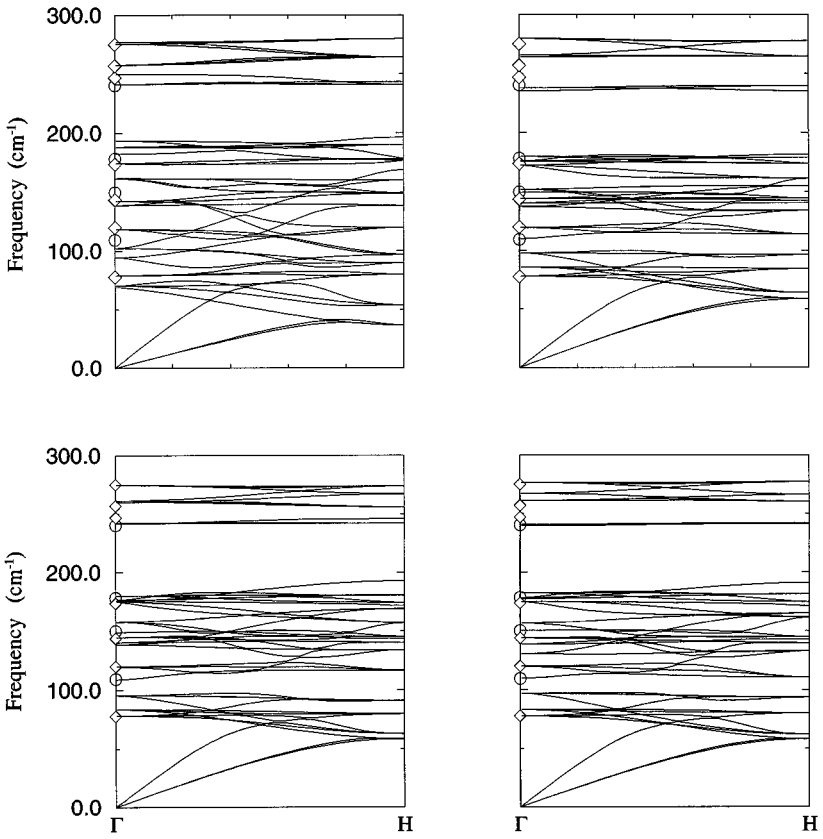

FIG. 4. Dispersion along Γ-H. The four models represented are LK (upper left), *A* (lower right), *B* (upper right), and *C* (lower left). The diamonds denote the infrared results of Ref. 8 and the circles denote our LDA results.

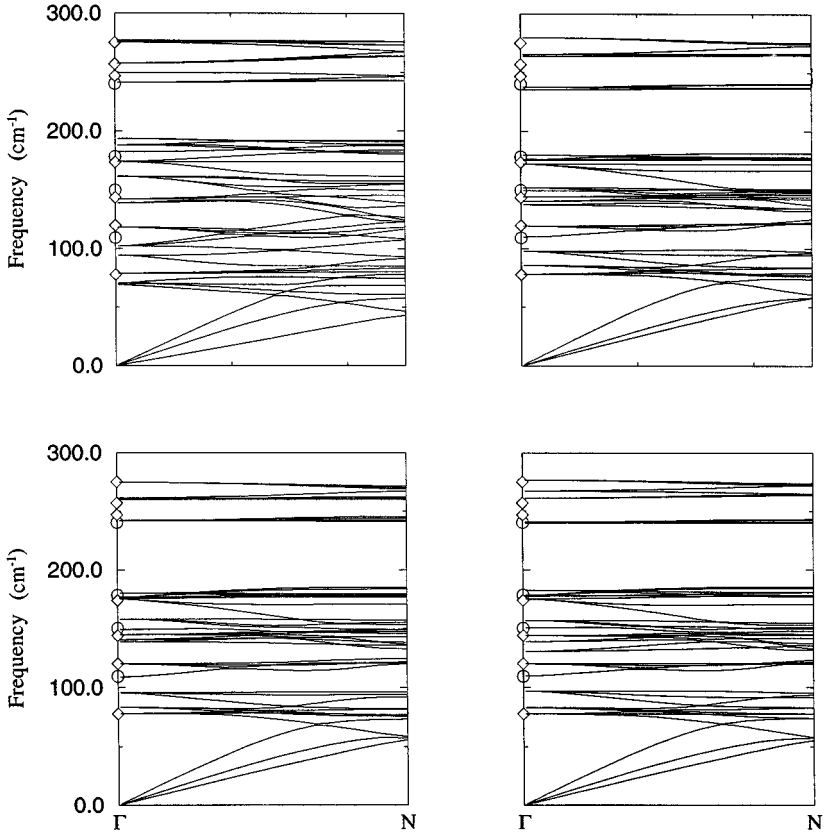

FIG. 5. Dispersion along Γ-N. See Fig. 1 caption.

side, respectively. Upon noticing the insignificant off-diagonal cubic terms, we set these to zero and instead added two diagonal quartic anharmonic parameters thereby keeping the number of parameters fixed. This resulted in a closer fit (a factor of 2 improvement in the standard and maximum deviations was obtained) and altered the quadratic coefficients by at most about 4%. However, the values of the two quartic parameters were disparate and the improvement in the fit is not clearly of significance. Finally, it is interesting to note that if central forces for pairs of Sb atoms along the rectangles' sides dominated the effect of the remaining interatomic forces in the A_g symmetry distortional energy then the qualitative results of Table I would be obtained. Namely, the cross terms in both harmonic and anharmonic sets of coefficients are small, and (as can be shown) the diagonal parameters of largest magnitude represent stretching of the shortest side of each rectangle. Our numerical results, the small Sb separations, and the LK lattice-dynamical analysis of infrared data all point to the existence of strong central interactions between neighboring Sb atoms constituting the four-membered rings.

D. A_u symmetry displacements

Similarly to the A_g symmetry case, two independent A_u symmetry coordinates q_i exist.[14] However, an A_u symmetry displacement (see Fig. 3) destroys the inversion symmetry of the crystal, so the crystalline energy must be an *even* function of the A_u symmetry coordinates if all other coordinates are set to zero. With the neglect of quartic and higher-order anharmonic terms, a minimum of three calculations of the total energy is required to obtain the appropriate dynamical matrix elements. We performed calculations for four sets of atomic displacements $\mathbf{u}_i$ consistent with A_u symmetry, and carried out a least-squares analysis. Specifically, if $\mathbf{e}_1(i)$ and $\mathbf{e}_2(i)$ represent normalized A_u basis vectors, where i runs over the basis atoms, then $\mathbf{u}_i = q_1\mathbf{e}_1(i)/m_i^{1/2} + q_2\mathbf{e}_2(i)/m_i^{1/2}$. With this definition, the coefficients of $q_iq_j/2$ in the energy expression are the dynamical matrix elements. Unlike the calculations of Sec. II C, the displacements from equilibrium were chosen to be extremely small, and it is justifiable to ignore quartic anharmonic coefficients in the least-squares analysis. The fit was good to better than 2 μRy deviations which is considered to be well within the accuracy of our LDA calculations. Diagonalization of the resulting matrix yielded values 109.5 and 240.5 cm^{-1} for the normal mode frequencies. The lower frequency mode is characterized by comparable magnitudes of Sb and Co displacements as well as ''in-phase'' motion of nearest-neighbor Sb and Co atoms and the higher frequency mode by primarily Co motion and ''out-of-phase'' motion of nearest-neighbor Sb and Co atoms. (Since the Sb and Co motions are not collinear it is necessary to loosely define relative phase through projections along interatomic vectors.)

III. FORCE-CONSTANT MODELS

A. Lutz-Kliche model

Lutz and Kliche (LK) fitted six central bond-stretching force constants to seven infrared-active modes. They included the nearest-neighbor Co-Sb interaction, of force con-

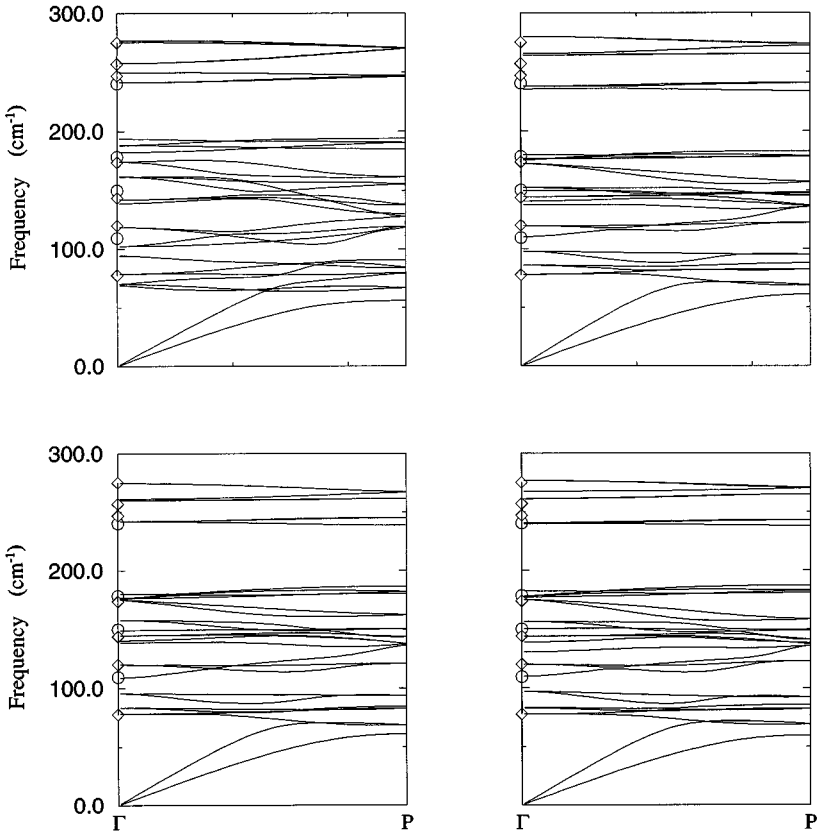

FIG. 6. Dispersion along Γ-P. See Fig. 1 caption.

stant a_1, the nearest-neighbor Co-Co interaction, of force constant a_2, the two nearest-neighbor Sb-Sb interactions within the rectangles, of force constants a_3 and a_4, and the two nearest-neighbor Sb-Sb interactions between rectangles, of force constants a_5 and a_6. Ionic Coulomb forces were ignored and are probably not strong contributors to the lattice dynamics of $CoSb_3$. We have used their model to compute all the other zone-center frequencies and the dispersion curves and have also used it to compute the volume dependence for comparison with our LDA results. Indeed it is remarkable how well their model predicts the LDA volume dependence of the total energy, as shown (Fig. 2), as well as both A_g mode frequencies, and the uppermost A_u frequency for which we found the LK model to yield 162, 183, and 250 cm^{-1}, respectively. Where we found the model to fail was in the low-frequency A_u mode, as the LK model gives 69 cm^{-1} for this mode. The low-frequency A_u mode involves a large twist of the Sb rectangles (see Fig. 3) and a concerted motion between Co and Sb atoms such that the interatomic distance changes between neighboring Co and Sb atoms tend to be minimized. This displacement pattern implies that the strong bond-stretching forces are unimportant for the mode and that instead longer range and/or bond-angle forces are important. Of course, the LK model does not contain bond-angle force constants.

B. Extended Lutz-Kliche model

Although bond-angle restoring forces are not included in the LK model, the basic success of the model was very encouraging, and we attempted to simply refit its parameters using all of the available zone-center mode frequencies, i.e., infrared data and LDA results. However, we were unsuccessful in the sense that unreasonable values of the force constants were obtained. For example, pairs of atoms that might be expected to be similarly bonded such as the two nearest-neighbor Sb atoms were found to have order of magnitude differing force-constant values. Therefore we decided to look for a model with a slight increase in the number of parameters.

Covalent bonding is clearly important in this material, for the strongly hybridized band structure gives no indication of ionicity and the material is a covalent semiconductor albeit with a small energy gap.[5] For this reason and the above empirical reason, force-constant parameters associated with bond-angle distortions have been taken into account in our development. Our goal was to find a single type of interaction to be added to the LK model that simultaneously produced a good fit to all of the frequency ''data'' and reasonable values of the force constants, and we considered bond-bending force constants (arising from pair potentials when equilibrium interatomic distances differ from the positions of the pair potential minima) and Sb-Co-Sb bond-angle force constants. However, neither of these additions gave physically reasonable results and therefore they were not considered further. Instead, Sb-Sb-Co bond-angle force constants were found to give good results. These have two possibly distinct values, corresponding to atoms 1-8-6 and 1-11-15 in Fig. 3. They also seemed to be a natural choice because the corresponding equilibrium bond angles of 109.2° and 107.8° are close to the tetrahedral angle (109.47°), and in materials

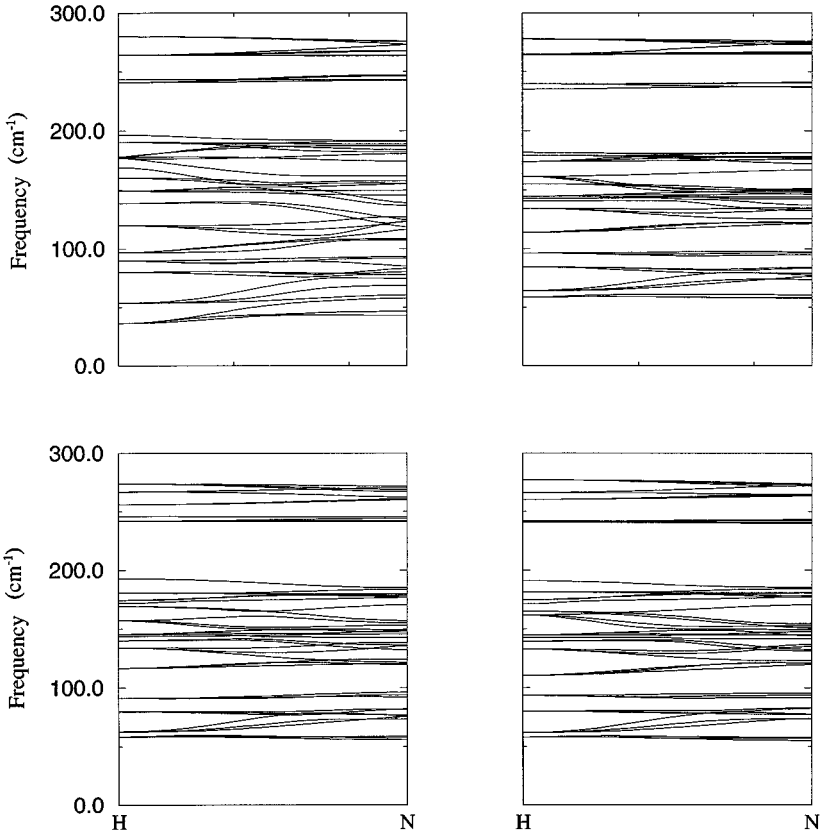

FIG. 7. Dispersion along *H-N*. See Fig. 1 caption.

of diamond or zinc-blende structures bond-angle terms in the energy seem to be of great importance. The model which we have developed and for which numerical results are presented in the remainder of this paper consists of (a) the LK-type bond-stretching parameters, (b) two bond-angle terms, with parameters a_7 and a_8, associated with the above two distinct Sb-Sb-Co bond angles, and (c) a single additional stretching force constant (denoted a_9) between second- and third-neighbor Co and Sb atoms (pairs 1–12 and 1–15 in Fig. 3). The addition (c) was made primarily to improve the accuracy of the model with respect to the LDA results for the A_u polarization vectors. It is also reasonable to include these Co-Sb interactions, for the interatomic distances involved are 4.39 and 4.45 Å, which are both less than the Co-Co interatomic distance included in the LK model. On the other hand, we have not explored in any detail the effect of an interaction between Sb atoms along the diagonals of the rectangles, although that length is only 4.12 Å.

The parameters of our model are denoted a_i with $i=1-6,9$ for bond-stretching force constants and $i=7,8$ for bond-angle energy parameters:

$$U_3=\sum_{i=7}^{8}\sum_{(l>m>n)_i} a_i(\cos\theta_{l,m,n}-\cos\theta_i)^2. \qquad (2)$$

Here θ_i is an equilibrium bond angle, the indices l, m, and n label the atoms, and the i subscript on $l>m>n$ denotes the constraint to triplets of a particular kind [$i=7,8$ correspond to all triplets symmetrically equivalent to 1-8-6, 1-11-15 of Fig. 3(a)]. The dynamical matrix contribution results from expanding this expression and keeping only quadratic terms in powers of atomic displacements. Group theory was applied with the help of the paper by Boyer[15] and for zone-center modes the dynamical matrix was written as a function of the a_i's and associated block diagonal matrices. Least-squares fits (to the 11 known zone-center frequencies) were made to a_i with $i=1,7$, with $a_8/a_7(=r_1)$ and $a_9/a_1(=r_2)$ kept fixed, thereby formally adding one least-squares fitted parameter and four data points to the quantities used by LK. Finally, upon achieving reasonable models based on the frequencies alone, we compared our model results for the bulk modulus and A_g and A_u polarization vectors to our LDA results. We present results based on four pairs of values of r_1 and r_2, each of which gave satisfactory results for all the infrared and LDA quantities. These constitute the four sets of model parameters of this study.

IV. RESULTS OF MODELS

A. Force-constant parameters, elastic constants, and zone-center normal modes

Table II shows the values of the parameters obtained and Table III the fits to the normal mode frequencies on which those values are based. Models *A*, *B*, *C*, and *D* correspond to LK-type force constants with the addition of cosine terms for Sb-Sb-Co bond angles and additional Sb-Co stretching force constants as discussed above. It should be noted that $a_7(a_8)$ is associated with the bond angle 109.2° (107.8°) and with the Sb-Sb interatomic distance 2.86 Å (2.97 Å). Except perhaps for the ratio between a_6 and a_5 our models (*A*–*D*)

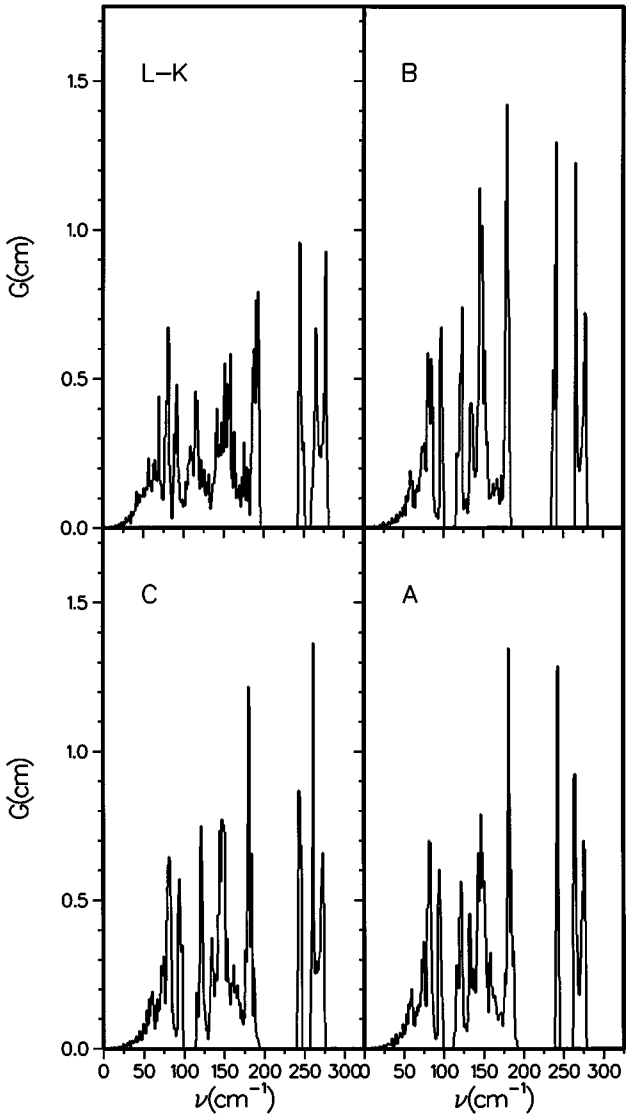

FIG. 8. Phonon density of states. The models represented are indicated in the separate panels. The normalization for the curves is 48.

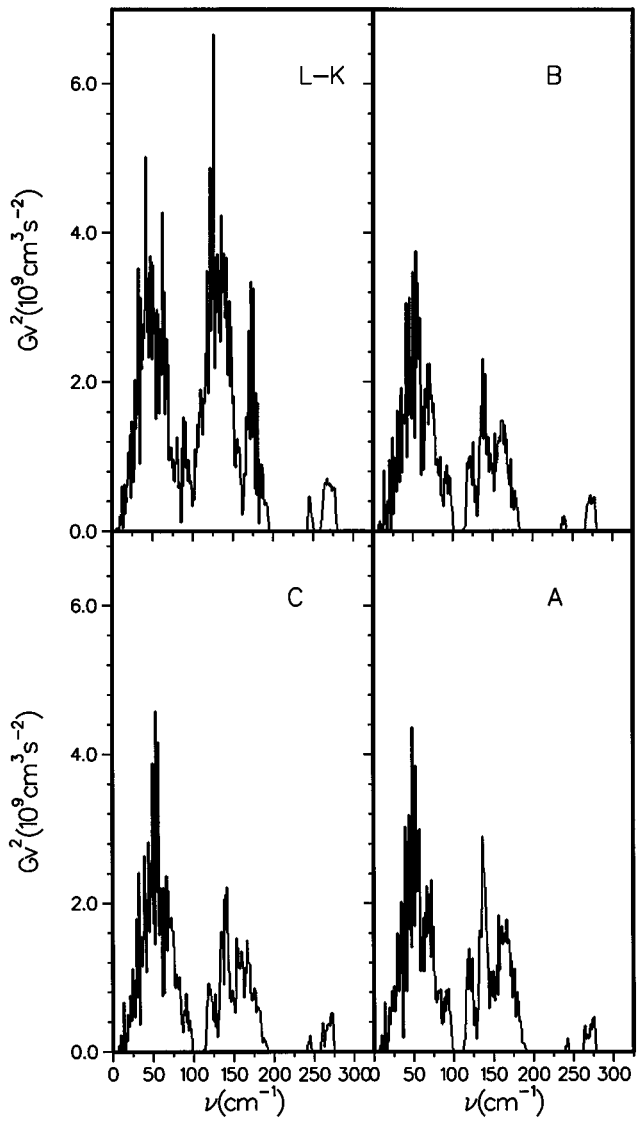

FIG. 9. Frequency averaged value of the square of the mode group velocities. As in Fig. 8 the models represented are indicated in the separate panels and the normalization for G is 48.

give comparable values of the bond-stretching parameters to that of LK, also represented in the table for comparison. For the models (C and D) in which the two bond-angle parameters are set equal to each other the angle terms are found to have the largest values, and the deviation from the LK model is greatest.

Elastic constant values are also presented in Table II. The effects of changes in internal parameters in the presence of the appropriate elastic strain give ''relaxational'' contributions to the elastic constants. The unrelaxed bulk modulus for the force-constant models can be directly compared to the LDA value of 105 GPa which was not used in the fits, and the agreement is quite satisfactory since generally one expects LDA bulk moduli to be good to within 5 or 10 %. It is also shown in Table II that only a small relaxational effect in the bulk modulus occurs within the models. The quantity c' is defined as $(c_{11}-c_{12})/2$ and the difference between c_{44} and c' represents the predicted elastic anisotropy which, for our models, is of a magnitude found in many cubic materials. The unrelaxed values of c_{44} are comparable for all of the models, so the small LK value in Table II arises from a large—50% of the unrelaxed value—relaxational contribution for the model compared to those of our models which are about 15% of the unrelaxed values. The elastic constant Debye temperature was evaluated using de Launay's tables.[16] The values shown are substantially smaller than the values estimated from an analysis of thermal conductivity measurements and a sound velocity measurement, which are 287 and 306 K, respectively.[5]

Our models (A–D) yielded a good fit to all 11 available frequencies and comparable fits to the infrared frequencies were obtained for all of the models (LK and A–D). The largest deviation from any of the infrared modes occurs for model B and the mode at 247 cm^{-1}, where the discrepancy is about 9 cm^{-1} and it is noted that this is the infrared mode that all of the models fit poorest. Overall, for the infrared modes, models D and B give the poorest fits to the data as they depart from the data by more than 3 cm^{-1} for one and two additional modes, respectively. None of the models gives excellent agreement with the LDA polarization vectors. A

TABLE V. LDA and model polarization vectors (A_g and A_u modes). Only the lower eigenvalue solution (see Table III) is shown in each case. The others are obtained from the orthogonality requirement.

		LK	*A*	*B*	*C*	*D*	LDA
A_g	e_x(Sb-11), [a]	−0.996	−0.990	−0.976	−0.987	−0.974	0.995
	e_y(Sb-11)	0.087	0.142	0.217	0.159	0.227	0.098
A_u	$e_x=e_y=e_x$(Co-1)[a]	0.609	0.568	0.504	0.579	0.515	0.438
	e_x(Sb-9)	0.793	0.823	0.864	0.815	0.857	0.899

[a]The atom numbers and Cartesian coordinates refer to those of Fig. 3 and a polarization vector normalization of 12 has been used. Atomic displacements are given by $m_i^{-1/2}\mathbf{e}(i)$; $i=1,16$.

stronger force constant a_9 is seen to improve the agreement for the A_u mode but destroys the agreement for A_g mode and it is seen that the sign of the small component of the A_g polarization vector is given incorrectly by all of the models (Table V).

In addition to the low-frequency A_u mode, only the low-frequency E_u mode (see Table IV) is in serious discrepancy between our models and the LK model, although the more than 10% discrepancy for the low-frequency F_g mode is also worth mentioning especially since it is a Raman-active mode. While we have not performed a parallel analysis, we have examined the zone-center modes in detail and found that the highest-frequency modes consist primarily of Co motions and the lowest, primarily of rigid-rectangle Sb motions.

B. Dispersion and group velocities

In this and the remaining portion of the paper we shall omit results based on model *D* for convenience of presentation. The dispersion curves along symmetry directions are given in Figs. 4 thru 7. Models *A*–*D* are practically identical on the scale of the differences between them and the LK model. The main difference between the LK model and our models is that the dispersion is greater throughout the zone for the LK model than for our models: It is possible to *follow* a particular curve from the acoustic branch throughout some of the optical branches within the LK model. It is somewhat surprising that the difference in dispersion curves should be large between our and LK's models since there is not a great difference between the nature of the models.

The phonon densities of states are presented in Fig. 8. They were obtained from a sampling of 256 points in the irreducible element of the Brillouin zone. It is noteworthy that with the exception of the LK spectrum, which has no low-frequency gap, all the spectra have a gap between ~ 100 and ~ 110 cm^{-1}. An unusual feature of the spectra, at ~ 70 cm^{-1}, is the sudden departure from the low-frequency parabolic behavior. As seen in the dispersion curves there are optic branches with frequencies of this magnitude, thereby giving rise to the departure from parabolic behavior. It is also of interest to characterize the modes. Lutz and Kliche have discussed the infrared-active modes in terms of force-constant distributions and one can gain some insight into the mode characteristics from such an analysis. While we have not performed their analysis, it is apparent that certain optic modes (~ 70 cm^{-1}) have rather rigid rectangle behavior, others have Sb-Sb bond-bending (~ 110 cm^{-1}) and bond-stretching (~ 150–175 cm^{-1}) behaviors, and others large Co motion (~ 250 cm^{-1}). It is tempting to characterize the various peaks seen in the spectra in such a manner.

In view of the importance of understanding thermal conductivity, we have plotted a histogram of $\langle v^2\rangle G$ in Fig. 9 where $\mathbf{v}_i$ is the group velocity for each normal mode and the average is a weighted average over the Brillouin zone with weighting factor $\delta(\nu-\nu_i)$, where ν_i is the normal mode frequency of mode i, $\mathbf{v}_i$ is calculated by taking the wave-vector derivative of the dynamical matrix. This function merely gives a qualitative understanding of what modes might contribute to the thermal conductivity, as similar quantities (we have not distinguished between transverse and longitudinal modes, for example) enter a relaxation time approximation to the Boltzmann-Peierls theory of thermal conductivity. $\langle v^2\rangle G$ is seen to be appreciable for optic mode frequencies as well as acoustic ones but this effect is much less pronounced for our models than for the LK model. In particular, it appears that those optic modes associated with substantial Sb motion and in particular rigid rectangle motion may play an important role in thermal conduction.

C. Cubic anharmonic potential

The cubic anharmonic information in these LDA calculations is the volume dependence of the bulk modulus and A_g mode interactions. Our force model study of anharmonicity was limited to the following: We have added a cubic anharmonic term, $-(1/6)(10a_i/r_0)(r-r_0)^3$ to a parabolic term $(1/2)a_i(r-r_0)^2$ for each central force constant a_i in model *C*. This yielded (in 10^{-4} Ry/unit cell) 3.2, −4.9, 0.024, and 0.088 for the terms a_{uuu}, a_{vvv}, a_{uuv}, and a_{uvv}, respectively. The agreement with the results of Table I is excellent. In addition, the same factor of 10 represents the anharmonicity in the volume-dependent LDA results very well. For comparison, the repulsive term ($\sim 1/r^{12}$) in the Lennard-Jones potential corresponds to a factor of 14 relating the cubic and quadratic terms, although we do not suggest a Lennard-Jones potential for closely representing the interactions of our model. Furthermore, the same factor (10) used to derive the above potential was found to be appropriate for representing the volume dependence of the energy.

V. DICUSSION AND SUMMARY

In this work, first-principles calculations have been incorporated into a lattice-dynamical force-constant fit of experimental (infrared) and theoretical results for normal mode frequencies and in an estimate of anharmonic parameters. This is in a similar spirit to studies by Vanderbilt, Taole, and

Narasimhan[17] for silicon and by Ye *et al.*[18] for molybdenum. The calculation of the A_u frequencies was very crucial to our understanding of the lattice dynamics since it provided the only indication of the limitation of the previous Lutz-Kliche force-constant model. A covalent angle force-constant was found to be necessary, of course, within only a limited investigation, for achieving a reasonable model that agreed with the known frequencies. The need for including such a term in this analysis is consistent with a covalent bonding picture for the skutterudites as indicated by band-structure results. The (constrained) bulk modulus has also been given accurately by those models, although the bulk modulus was not directly used in the fitting procedure. The agreement in the eigenvectors, also not fit, between the LDA and the models is somewhat unsatisfactory (see Table V) for both the A_g and A_u modes. Nevertheless, we have obtained the phonon dispersion curves, phonon density of states, and a group velocity average that is *related* to thermal conductivity and found these to be rather model independent (except for the difference between the LK model and our models) using models that give different results for these polarization vectors. We have also made predictions for elastic constants and the low-temperature Debye temperature. A factor-of-two discrepancy in c_{44} is found between our models and the earlier (LK) model. The values we obtain for the Debye temperature differ greatly from quoted values in the literature estimated from thermal conductivity measurements and a sound velocity measurement. Complete single-crystal elastic constant measurements, Raman scattering, neutron-scattering or low-temperature specific heat measurements would be valuable in checking our models. Finally, based on the small extracted cross terms (both harmonic and anharmonic) in the expansion in powers of the internal structural parameters, u and v, we assert that central, bond-stretching interactions are the dominant intrarectangle interactions.

Note added in proof. Several of the Raman active modes have been measured and reported on in a recent article by G. S. Nolas, G. A. Slack, T. Caillat, and G. P. Meisner [J. Appl. Phys. (to be published)], and the results are in reasonably good agreement with our predictions.

ACKNOWLEDGMENTS

We thank G. Slack, G. Nolas, and L. Nordstrom for stimulating conversations and M. Mehl for assistance with the phonon density-of-states calculation. This work was supported by ONR and the DOD computer centers at CEWES and NAVO.

[1] G. A. Slack, in *Solid State Physics: Advances in Research and Applications*, edited by H. Ehrenreich, F. Seitz, and D. Turnbull (Academic, New York, 1979), Vol. 34, p. 1.

[2] T. Caillat, A. Borshchevsky, and J. P. Fleurial, in *Proceedings of the Eleventh International Conference on Thermoelectricity, Arlington, Texas*, edited by K. R. Rao (University of Texas at Arlington Press, Arlington, 1993).

[3] G. A. Slack and V. G. Tsoukala, J. Appl. Phys. **76**, 1665 (1994).

[4] D. T. Morelli, T. Caillat, J. P. Fleurial, A. Borshchevsky, J. Vandersande, B. Chen, and C. Uher, Phys. Rev. B **51**, 9622 (1995).

[5] D. J. Singh and W. E. Pickett, Phys. Rev. B **50**, 11 235 (1994).

[6] D. T. Morelli and G. P. Meisner, J. Appl. Phys. **77**, 3777 (1995).

[7] G. S. Nolas, G. A. Slack, T. M. Tritt, and D. T. Morelli (unpublished).

[8] H. D. Lutz and G. Kliche, Phys. Status Solidi B **112**, 549 (1982).

[9] The nearest-neighbor distance between Co and Sb atoms is 2.54 Å, and the next-nearest-neighbor distances between Sb's along the sides of the rectangles are 2.85 and 2.97 Å. Inter-rectangle nearest-neighbor distances between Sb atoms are 3.43 and 3.71 Å.

[10] D. Singh, Phys. Rev. B **43**, 6388 (1991).

[11] O. K. Andersen, Phys. Rev. B **12**, 3060 (1975).

[12] D. J. Singh, *Planewaves Pseudopotentials and the LAPW Method* (Kluwer, Boston, 1994); and references therein.

[13] L. Hedin and B. I. Lundqvist, J. Phys. C **4**, 2064 (1971).

[14] H. D. Lutz and G. Kliche, Z. Anorg. Allg. Chem. **480**, 105 (1981).

[15] L. L. Boyer, J. Comp. Phys. **16**, 167 (1974).

[16] J. De Launay, J. Chem. Phys. **30**, 91 (1959).

[17] D. Vanderbilt, S. H. Taole, and S. Narasimhan, Phys. Rev. B **40**, 5657 (1989-I); **42**, 11 373 (1990-I).

[18] Y. Y. Ye, H. K. Ho, Y. Chen, and B. N. Harmon, J. Phys. Condens. Matter **3**, 9629 (1991).